Research in Astronomy and Astrophysics, 24:055012 (11pp), 2024 May https://doi.org/10.1088/1674-4527/ad3c70

The Multi-parameter Test of Gravitational Wave Dispersion with Principal Component Analysis

Zhi-Chu Ma[1,2], Rui Niu[1,2], and Wen Zhao[1,2]
[1] CAS Key Laboratory for Research in Galaxies and Cosmology, Department of Astronomy, University of Science and Technology of China, Hefei 230026, China; nrui@mail.ustc.edu.cn
[2] School of Astronomy and Space Sciences, University of Science and Technology of China, Hefei 230026, China
Received 2024 January 31; revised 2024 March 27; accepted 2024 April 5; published 2024 May 10

Abstract

In this work, we consider a conventional test of gravitational wave (GW) propagation which is based on the phenomenological parameterized dispersion relation to describe potential departures from General Relativity (GR) along the propagation of GWs. But different from tests conventionally performed previously, we vary multiple deformation coefficients simultaneously and employ the principal component analysis (PCA) method to remedy the strong degeneracy among deformation coefficients and obtain informative posteriors. The dominant PCA components can be better measured and constrained, and thus are expected to be more sensitive to potential departures from the waveform model. Using this method we analyze ten selected events and get the result that the combined posteriors of the dominant PCA parameters are consistent with GR within 99.7% credible intervals. The standard deviation of the first dominant PCA parameter is three times smaller than that of the original dispersion parameter of the leading order. However, the multi-parameter test with PCA is more sensitive to not only potential deviations from GR but also systematic errors of waveform models. The difference in results obtained by using different waveform templates hints that the demands of waveform accuracy are higher to perform the multi-parameter test with PCA. Whereas, it cannot be strictly proven that the deviation is indeed and only induced by systematic errors. It requires more thorough research in the future to exclude other possible reasons in parameter estimation and data processing.

Key words: gravitational waves – gravitation – black hole physics

1. Introduction

General Relativity (GR) is considered as the most successful gravity theory which has been intensively tested in the past across scales of laboratory experiments to observations of the large-scale structure of the universe (Adelberger 2001; Hoyle et al. 2001; Stairs 2003; Jain & Khoury 2010; Wex 2014; Will 2014; Berti et al. 2015; Manchester 2015; Koyama 2016; Kramer 2017). However, on the theoretical side, difficulties in problems of singularity and quantization (DeWitt 1967; Kiefer 2007) hint at the possible incompleteness of GR. On the observational side, to explain current observations of galaxies and cosmology within the framework of GR, conceptions like dark matter and dark energy have to be introduced (Frieman et al. 2008; Porter et al. 2011), while there is another possibility that GR might be invalid at this scale (Debono & Smoot 2016). These facts continuously motivate people to pursue higher precision or develop new methods for performing tests on GR. In recent years, gravitational wave (GW) observations provide an unprecedented way to test GR.

The direct detection of the binary black hole coalescence event, GW150914 (Abbott et al. 2016a), initiated the era of GW astronomy. More than 90 GW events from compact binary coalescence have been detected (Abbott et al. 2019a, 2021; Collaboration et al. 2021a, 2023) in the three previous observing runs of the LIGO, Virgo, and KAGRA collaboration (LVK). Thorough tests on GR have been performed by LVK based on these detected GW data (Collaboration et al. 2021, 2023, 2021c).

The tests performed by LVK include three aspects of GWs: generation, propagation, and polarization. The methods used can be classified as consistency tests and parameterized tests (Collaboration et al. 2021, 2023, 2021c). Consistency tests aim at checking whether the observed data are consistent with predictions of GR, such as the residual test where the best-fit waveform will be subtracted from data and checking whether there is remnant coherent power in residuals (Cornish & Littenberg 2015), or the inspiral-merger-ringdown consistency test where the low frequency and high frequency parts of signals are used to perform parameter estimation separately and checking whether the results are consistent (Ghosh et al. 2016, 2017). In addition, parameterized tests adopt specific parameterization of possible deviations from GR. For example, the parameterized test of GW generation (Li et al. 2012; Agathos et al. 2014) utilizes the parameterization based on the

post-Newtonian (PN) expansion structure. Deformation coefficients are added to original PN coefficients which are solely determined by masses and spins of the binary in GR. The additional deformation coefficients will be estimated as free parameters in Bayesian parameter estimation, which can capture various possible unmodeled effects and can also be mapped to modifications in specific alternative gravity theories through the parameterized post-Einsteinian (ppE) framework (Yunes & Pretorius 2009). Similarly, the parameterized dispersion relation is used in the test of GW propagation (Mirshekari et al. 2012). Additional power terms of GW momentum are added in the dispersion relation, which can make different frequency components of GWs propagate with different speeds, thus distorting the observed waveform (Will 1998; Mirshekari et al. 2012).

There are multiple deformation coefficients in parameterized tests for capturing various potential deviations. Due to the limitation of sensitivity of current detectors, if varying all deformation coefficients simultaneously in parameter estimation, correlations among parameters will lead to uninformative posteriors. Thus, in tests performed by LVK, only one deformation parameter is allowed to vary at a time (Abbott et al. 2016b, 2019b; Collaboration et al. 2021, 2023, 2021c).

However, in the most general and agnostic-priori case, all deformation parameters need to be considered as free parameters in Bayesian inference. The class of parameterized tests where multiple deformation parameters are constrained simultaneously is referred to as multi-parameter tests (Datta et al. 2021; Gupta et al. 2020; Saleem et al. 2022). Previous works (Datta et al. 2021; Gupta et al. 2020) show that the multi-band observations by third-generation ground-based detectors and space-borne detectors can allow people to perform multi-parameter tests and get tight constraints on PN deformation coefficients. Another approach to perform multi-parameter tests is employing the method of Principal Component Analysis (PCA) to reduce correlations among parameters and get informative posteriors (Pai & Arun 2012; Ohme et al. 2013; Saleem et al. 2022; Datta et al. 2024; Datta 2023; Shoom et al. 2023). The previous work (Saleem et al. 2022) applies this method in the parameterized test of GW generation. In this work, we will extend this method to the parameterized test of GW propagation. The rest of this paper is organized as follows. In Section 2, we introduce the parameterized test of GW propagation, and the method of PCA for multi-parameter tests. We apply this method to 10 selected GW events, and present results in Section 3. The summary is shown in Section 4.

2. Methods

2.1. The Multi-parameter Test of GW Propagation

The main effort of this paper is extending the multi-parameter test of GW generation with PCA performed in the previous work (Saleem et al. 2022) to the test of propagation. We focus on the effects of dispersion, while other propagation effects like birefringence (Zhao et al. 2020; Wang et al. 2021b; Okounkova et al. 2021; Niu et al. 2022; Wang et al. 2022) or amplitude damping (Belgacem et al. 2018; Nishizawa 2018) are not included in this paper. The test of propagation considered here is based on the phenomenological modified dispersion relation (Mirshekari et al. 2012) which reads

$$E^2 = p^2 + \sum_\alpha A_\alpha p^\alpha, \tag{1}$$

where E and p are the energy and momentum of GW respectively, A_α are the free parameters for capturing various potential deviations from GR, and α values correspond to modifications at different frequency orders. When $A_\alpha = 0$ for all α, this modified dispersion relation returns to the case of GR. Leading-order modifications in various alternative theories can be mapped to the terms with different values of α (Yunes & Pretorius 2009; Mirshekari et al. 2012; Yunes et al. 2016).

This phenomenological modified dispersion relation is a generic framework and can cover a wide variety of alternative theories, where the behaviors of GW propagation are different from GR, including theories with massive gravitons or various Lorentz-violating alternative gravity theories (Mirshekari et al. 2012). For example, the case of $\alpha = 0$ and $A_0 > 0$ corresponds to deformations induced by massive gravitons (Will 1998); the leading-order corrections in multi-fractal spacetime (Calcagni 2010) and the doubly special relativity (Amelino-Camelia 2002) can be mapped to the term of $\alpha = 2.5$ and 3; The Horăva–Lifshitz theory (Hořava 2009), extra-dimensional theories (Sefiedgar et al. 2011), and the standard model extension where if only non-birefringent effects are considered (Kostelecký & Mewes 2016), have leading modifications with $\alpha = 4$.

Additional power terms of momentum in the modified dispersion relation will make different frequency components of GW propagate with different speeds, thus leaving imprints in the waveform observed. Assuming the waveform in the local wave zone is consistent with GR, the additional corrections in phase induced by dispersion effects along propagation are given by Mirshekari et al. (2012)

$$\delta\Phi_\alpha(f) = \mathrm{sign}(A_\alpha)\begin{cases} \dfrac{\pi(1+z)^{\alpha-1}D_\alpha}{\alpha-1}\lambda_\alpha^{\alpha-2} f^{\alpha-1}, & \alpha \neq 1, \\ \dfrac{\pi D_\alpha}{\lambda_\alpha}\ln(\pi\mathcal{M}f), & \alpha = 1. \end{cases} \tag{2}$$

In the above equation, $\mathcal{M}$ is the chirp mass of the binary, and $\lambda_\alpha = h|A_\alpha|^{1/(\alpha-2)}$ with the Planck constant h, D_α is defined as

$$D_\alpha = \frac{(1+z)^{1-\alpha}}{H_0}\int_0^z \frac{(1+z')^{\alpha-2}}{\sqrt{\Omega_{\mathrm{m}}(1+z')^3 + \Omega_\Lambda}}dz', \tag{3}$$

where H_0 is the Hubble constant, z is the redshift of the source, and Ω_m and Ω_Λ are the matter and dark energy density parameters respectively. We use the values reported in Planck 2018 results (Aghanim et al. 2020), where $H_0 = 67.66\,\mathrm{km\,s^{-1}\,Mpc^{-1}}$, $\Omega_m = 0.3111$ and $\Omega_\Lambda = 0.6889$.

For the convenience of varying all deformation coefficients simultaneously in parameter estimation, we consider a parameterization which is slightly different from that used by LVK (Abbott et al. 2016b, 2019b; Collaboration et al. 2021, 2023, 2021c). Dimensionless coefficients

$$\delta\phi_\alpha = 1\ \mathrm{Gpc}(10^3\ M_\odot)^{1-\alpha}\lambda_\alpha^{\alpha-2}, \tag{4}$$

are constructed, where the factors of distance and mass in front are adjusted according to typical values of detected sources in order to scale the magnitude of deformation coefficients to a close order. Therefore, the phase correction of Equation (2) can be rewritten as

$$\delta\Phi_\alpha(f) = \mathrm{sign}(A_\alpha) \times \begin{cases} \delta\phi_\alpha \frac{(1+z)^{\alpha-1}}{(\alpha-1)\pi^{\alpha-2}} \left(\frac{10^3\,M_\odot}{M}\right)^{\alpha-1} \left(\frac{D_\alpha}{1\ \mathrm{Gpc}}\right) (\pi M f)^{\alpha-1}, & \alpha \neq 1, \\ \delta\phi_\alpha \frac{D_\alpha}{1\ \mathrm{Gpc}} \pi \ln(\pi \mathcal{M} f), & \alpha = 1. \end{cases} \tag{5}$$

The above modifications are added into a GR waveform model as the template used in the Bayesian parameter estimation. The measurement of all free parameters in the template, including deformation coefficients of dispersion effects and source properties in GR, will be presented through posterior distributions obtained by the nested sampling (Skilling 2004, 2006) or the Markov chain Monte Carlo (MCMC) (Hastings 1970; Foreman-mackey et al. 2013) algorithms. The posterior samples of $\delta\phi_\alpha$, after marginalizing over GR parameters, are manipulated by the PCA method to reduce correlations among these coefficients and obtain informative posteriors. We will describe the above procedures in more detail in the following.

2.2. Bayesian Parameter Estimation with GWs

Next, we present a brief review of Bayesian parameter estimation for GW data (Abbott et al. 2020). The physical information is extracted from observations through the Bayesian framework which estimates the probability distributions of parameters $\boldsymbol{\theta}$ in the model M according to observed data $\boldsymbol{d}$. The measurement is encoded by posterior distributions $p(\boldsymbol{\theta}|\boldsymbol{d}, M)$. According to Bayes' theorem, the posterior is given by

$$p(\boldsymbol{\theta}|\boldsymbol{d}, M) = \frac{p(\boldsymbol{\theta})p(\boldsymbol{d}|\boldsymbol{\theta}, M)}{p(\boldsymbol{d})}. \tag{6}$$

Here, $p(\boldsymbol{\theta})$ is the prior probability which reflects our prior knowledge of the parameters ahead of observations. The prior distributions of all parameters used in the parameter estimation are shown in Table 1. $p(\boldsymbol{d}|\boldsymbol{\theta}, M)$ is the likelihood whose value is the probability of the occurrence of a noise realization that is just equal to the observed data $\boldsymbol{d}$ subtracting a GW signal given by the model M with the specific values of $\boldsymbol{\theta}$. $p(\boldsymbol{d})$ is the normalizing factor and also is referred to as evidence for its usage in model selection.

Table 1
Priors Used in Parameter Estimation

Parameters	Priors
a_1	Uniform [0, 0.99]
a_2	Uniform [0, 0.99]
θ_1	Sine [0, π]
θ_2	Sine [0, π]
ϕ_{JL}	Uniform [0, 2π]
ϕ_{12}	Uniform [0, 2π]
ψ	Uniform [0, π]
δ	Cosine [$-\pi/2$, $\pi/2$]
α	Uniform [0, 2π]
θ_{JN}	Sine [0, π]
ϕ	Uniform [0, 2π]
$\delta\phi_0$	Uniform [−10, 10]
$\delta\phi_{2.5}$	Uniform [−800, 800]
$\delta\phi_3$	Uniform [−800, 800]
$\delta\phi_4$	Uniform [−500, 500]

Note. The notation follows symbols used in `Bibly` (Ashton et al. 2019; Romero-Shaw et al. 2020). For parameters of masses, luminosity distance, and merger time, we used uniform priors but the ranges are adjusted according to results published by LVK to reduce the computation burden of stochastic sampling. However, we believe enough large parameter spaces have been explored by ensuring that posteriors decline to zero at boundaries of priors. For waveform models of aligned spins, we use the uniform prior in the range of [−0.99, 0.99] for the magnitude of projection of spin onto the orbital angular momentum. And for the waveform model `NRSur7dq4`, we adjust the prior range of mass ratio and magnitude of spins for satisfying the requirements of the waveform model.

In the GW data analysis context, assuming the noise is Gaussian and stationary, the likelihood can be written as

$$p(\boldsymbol{d}|\boldsymbol{\theta}, M) \propto \exp\left[-\frac{(\boldsymbol{d}-\boldsymbol{h}|\boldsymbol{d}-\boldsymbol{h})}{2}\right]. \tag{7}$$

Here, $\boldsymbol{h}$ is the GW signal given by a set of parameters $\boldsymbol{\theta}$ in a specific model M, and the brackets denote the inner product which is defined as

$$(a|b) = 4\,\mathrm{Re}\int df \frac{a^*(f)b(f)}{S_n(f)}, \tag{8}$$

where $S_n(f)$ is the power spectral density (PSD) of detector noise. For GW signals, the dimension of parameter space is usually high, and the likelihood evaluation is usually computationally expensive. Computing posteriors on a grid is impractical. Stochastic sampling algorithms, including nested sampling (Skilling 2004, 2006) or the MCMC (Hastings 1970;

Foreman-Mackey et al. 2013), are used to obtain random samples whose densities can be approximated to the posterior probabilities.

In our situation, the model contains multiple dispersion parameters $\delta\phi_\alpha$ together with GR parameters. Different from tests performed by LVK, we vary multiple deformation parameters simultaneously in the parameter estimation introduced above. After marginalizing GR parameters, the posterior samples of dispersion parameters are manipulated by the procedure discussed in the next subsection to reduce correlations.

2.3. Principal Component Analysis

Different from the tests performed by LVK, multiple dispersion parameters are varied simultaneously in our parameter estimation. Due to correlations among these deformation parameters, varying multiple parameters will lead to less informative posteriors. However, previous works (Pai & Arun 2012; Ohme et al. 2013; Saleem et al. 2022; Datta et al. 2024; Datta 2023; Shoom et al. 2023; Niu et al. 2024) show that this problem can be remedied by the method of PCA.

The method of PCA will find a new set of bases for the parameter space by a linear combination of original parameters. The newly constructed parameters have reduced correlations, and can be better constrained by data. To obtain the new bases, we first need to compute the covariance matrix $\mathbf{\Sigma}$ for the posterior samples of dispersion parameters $\delta\phi_\alpha$ after marginalizing GR parameters, which is given by

$$\Sigma_{ij} = \langle(\delta\phi_i - \langle\delta\phi_i\rangle)(\delta\phi_j - \langle\delta\phi_j\rangle)\rangle. \tag{9}$$

Here, $\langle\cdots\rangle$ denotes the expectation value. Then, upon diagonalizing the covariance matrix $\mathbf{\Sigma}$, it can be written in terms of eigenvectors and eigenvalues as

$$\mathbf{\Sigma} = \boldsymbol{U}\mathbf{\Lambda}\boldsymbol{U}^T. \tag{10}$$

$\mathbf{\Lambda}$ is a diagonal matrix whose diagonal elements are eigenvalues of $\mathbf{\Sigma}$. $\boldsymbol{U}$ is a matrix composed by eigenvectors of $\mathbf{\Sigma}$. The eigenvectors are the new bases we are looking for, in which each dimension is linearly uncorrelated. The posteriors on this new set of bases can be obtained by the transformation

$$\delta\phi^{\rm PCA}_{i-{\rm th}} = \sum_j U^{ij}\delta\phi_j, \tag{11}$$

where $\delta\phi^{\rm PCA}_{i-{\rm th}}$ denotes the i-th principal component.

The levels signifying how principal a component is are indicated by the values of corresponding eigenvalues. The eigenvector with the smallest eigenvalue is the most dominant component corresponding to the new PCA parameter with the smallest error bar. The method of PCA redistributes the information on posteriors among the new bases, and collects information on all PN orders into dominant components. Therefore, potential deviations can be more obvious when consiering posteriors with their corresponding PCA parameters.

2.4. Combination of Results from Multiple Events

According to the method introduced above, we can perform the multi-parameter test of GW dispersion using a single GW event. In this subsection, we introduce the operation for combining information from multiple events.

The deviations from GR, if they exist, are believed to be universal for all events. Assuming the observation of each event is an independent measurement of deformation parameters $\delta\phi_\alpha$, we can directly multiply the posterior probabilities of $\delta\phi_\alpha$ given by each event to get the combined posteriors, which is the same process as in parameterized tests performed by LVK (Abbott et al. 2016b, 2019b; Collaboration et al. 2021, 2023, 2021c). However, since the linear combination of original dispersion parameters to get PCA parameters $\delta\phi^{\rm PCA}_{i-{\rm th}}$ is unique for each event, it is inappropriate to multiply posteriors of PCA parameters. Therefore, we resample the combined posteriors of $\delta\phi_\alpha$ and perform a separate operation of PCA to obtain the combined posteriors of $\delta\phi^{\rm PCA}_{i-{\rm th}}$.

In practice, we use Gaussian kernel density estimation (KDE) to obtain posterior probabilities of $\delta\phi_\alpha$ from its posterior samples for each event. Then, using a new MCMC sampling to sample the cumulative production of KDEs of all events, we can obtain the posterior samples of $\delta\phi_\alpha$ combining information from all events. The combined posteriors of PCA parameters $\delta\phi^{\rm PCA}_{i-{\rm th}}$ are obtained by performing a separate operation of PCA on the combined posterior samples of $\delta\phi_\alpha$

As will be discussed in the next section, to verify the robustness of using different waveform models, we do the same parameter estimation with different templates for each event. We rely on the method discussed in Ashton & Khan (2019) to average the results obtained by using different waveform approximations, where the posterior for a single event estimated by using a set of models M_i is given by

$$p(\boldsymbol{\theta}|\boldsymbol{d}, \{M_i\}) = \sum_i p(\boldsymbol{\theta}|\boldsymbol{d}, M_i)\xi_i, \tag{12}$$

and the weights ξ_i are defined as $\xi_i = Z_i/\sum_j Z_j$ with Z_i denoting the evidence of each waveform model.

3. Results and Discussions

We apply the method elaborated on in the last section to current observed GW data and present results in this section. Due to the limitation on sensitivity of current detectors, following the multi-parameter test of generation performed in Saleem et al. (2022), we also do not consider the full set of dispersion parameters. We only include the cases of $\alpha = 0$, 2.5, 3, and 4 in our analyses by considering the examples of leading order modifications in alternative theories mentioned in Mirshekari et al. (2012); Abbott et al. (2019c).

We analyze the 10 farthest events detected by LVK in three previous runs with criteria that the false alarm rate (FAR) is less than $10^{-3}\,{\rm yr}^{-1}$, the signal-to-noise ratio (S/N) greater than 12,

Table 2
The Information on 10 Selected Events Considered in Our Analyses

Name	$D_{\rm L}$ (Mpc)	S/N	FAR ($\rm yr^{-1}$)	$p_{\rm astro}$
GW170823	1940^{+970}_{-900}	$12.2^{+0.2}_{-0.3}$	$\leqslant 10^{-7}$	1.00
GW190408_181802	1540^{+440}_{-620}	$14.6^{+0.2}_{-0.3}$	$\leqslant 10^{-5}$	1.00
GW190503_185404	1520^{+630}_{-600}	$12.2^{+0.2}_{-0.4}$	$\leqslant 10^{-5}$	1.00
GW190512_180714	1460^{+510}_{-590}	$12.7^{+0.3}_{-0.4}$	$\leqslant 10^{-5}$	1.00
GW190513_205428	2210^{+990}_{-810}	$12.5^{+0.3}_{-0.4}$	1.3×10^{-5}	1.00
GW190519_153544	2600^{+1720}_{-960}	$15.9^{+0.2}_{-0.3}$	$\leqslant 10^{-5}$	1.00
GW190602_175927	2840^{+1930}_{-1280}	$13.2^{+0.2}_{-0.3}$	$\leqslant 10^{-5}$	1.00
GW190706_222641	3630^{+2600}_{-2000}	$13.4^{+0.2}_{-0.4}$	5.0×10^{-5}	1.00
GW190828_063405	2070^{+650}_{-920}	$16.5^{+0.2}_{-0.3}$	$\leqslant 10^{-5}$	1.00
GW190915_235702	1750^{+710}_{-650}	$13.1^{+0.2}_{-0.3}$	$\leqslant 10^{-5}$	1.00

Note. These events are 10 farthest events with criteria of FAR $< 10^{-3}$ $\rm yr^{-1}$, S/N > 12, and $p_{\rm astro} > 0.99$ in the Gravitational Wave Transient Catalog (GWTC). The values come from gwosc.org which may be different from the values shown in publications of LVK (Abbott et al. 2019a, 2021; Collaboration et al. 2021a, 2023).

and the probability of astrophysical origin ($p_{\rm astro}$) greater than 0.99. The potential dephasing caused by dispersion will accumulate along the propagation of GW. As can be seen through Equation (5), if the sensitivity to waveform dephasing $\delta\Phi_\alpha$ is fixed, we can generally constrain $\delta\phi_\alpha$ better by sources with farther distance. However, this is not strictly valid in any cases. The correlations among parameters are complicated, and the sensitivity to dephasing will depend on various factors, like S/N, and others. Only qualitatively can we expect that better constraints be obtained by further sources. The information on selected events is summarized in Table 2. We obtain strain data and noise PSD data from public data release of LVK.[3] The strain data with glitch subtraction are used in parameter estimation for events GW190503_185404 and GW190513_205428.

We use `bilby` (Ashton et al. 2019) with nested sampler `pymultinest` (Feroz & Hobson 2007; Feroz et al. 2008; Buchner et al. 2014) to perform Bayesian parameter estimation. Since the method of PCA is more sensitive to not only possible deviations from GR but also systematic errors of waveform template, we also use different waveforms, including `SEOBNRv4_ROM` (Pürrer 2014, 2015), `IMRPhenomXAS` (Pratten et al. 2020), `IMRPhenomXHM` (Pratten et al. 2021), and `NRSur7dq4` (Varma et al. 2019), in our parameter estimation.

The final results are presented in Figure 1 where the posteriors are obtained by averaging results of different waveform models with weights of evidence and combining results of all selected events using the method discussed in Section 2.4, and the results of each event are also shown in Figure 4. The posteriors of original dispersion parameters $\delta\phi_\alpha$ are shown on the left sides with blue shadow in each subplot, and posteriors of PCA parameters $\delta\phi^{\rm PCA}_{i-{\rm th}}$ are shown on the right sides with orange shadow. The blue and orange solid lines signify the 99.7% credible intervals, and the red dashed lines mean the GR values. Due to the limitation of plot ranges, the error bars of $\delta\phi^{\rm PCA}_{\rm 3rd}$, $\delta\phi_{2.5}$, $\delta\phi_3$, and the upper limit of $\delta\phi_0$ are out of the visible ranges. The explicit values of error bars and departures of maximum likelihood values from GR values are summarized in Table 3 for quantitative comparison.

We can observe that the posteriors of all parameters, including original dispersion parameters and PCA parameters, are consistent with GR within 99.7% credible intervals through Figure 1 and Table 3. As discussed in Section 2.3, the dominant PCA parameters can be better constrained, thus having smaller error bars, which are obviously shown in Figure 1 by observing the first three components. For example, the range of 99.7% credible intervals of the first dominant PCA parameter is 3 times smaller than that of the original dispersion parameter of the leading order. We can also notice that the maximum likelihood values are not exactly the GR values, which is reasonable considering unavoidable errors in waveform models and non-perfect Gaussian noise in reality. These departures are more obvious in dominant PCA parameters. Observing the subplot of the first dominant component $\delta\phi^{\rm PCA}_{0-{\rm th}}$ and the leading order dispersion parameters $\delta\phi_0$, the departure between the maximum likelihood value and the GR value of $\delta\phi^{\rm PCA}_{0-{\rm th}}$ is 2.85σ, while this value is 1.34σ for $\delta\phi_0$. This on one hand shows that the dominant PCA parameter is more sensitive to any departures in posteriors, and on the other hand indicates the demand of waveform accuracy is higher when searching for deviations using PCA.

The method of PCA is more sensitive to any departures from the considered waveform model, including both potential deviations from GR and systematic errors of the template or unmodeled effects. Therefore, we use different waveform models in parameter estimation and the obtained results are shown in Figures 2 and 3 for posteriors of original dispersion parameters and PCA parameters. From these two corner plots, we can find that, as introduced in Section 2.3, the new bases constructed by PCA have less correlations. Additionally, we can also observe that the results given by `IMRPhenomXPHM`, which is a phenomenological waveform model incorporating effects of higher modes and precession induced by in-plane spins, have slight differences from results produced by other waveform templates in terms of posteriors of original dispersion parameters. But after the operation of PCA, the result of `IMRPhenomXPHM` has obvious differences with others especially in the first dominant component. This in another aspect shows that the operation of PCA is sensitive to minor changes in posteriors of original parameters, which

[3] https://gwosc.org/eventapi/html/GWTC/

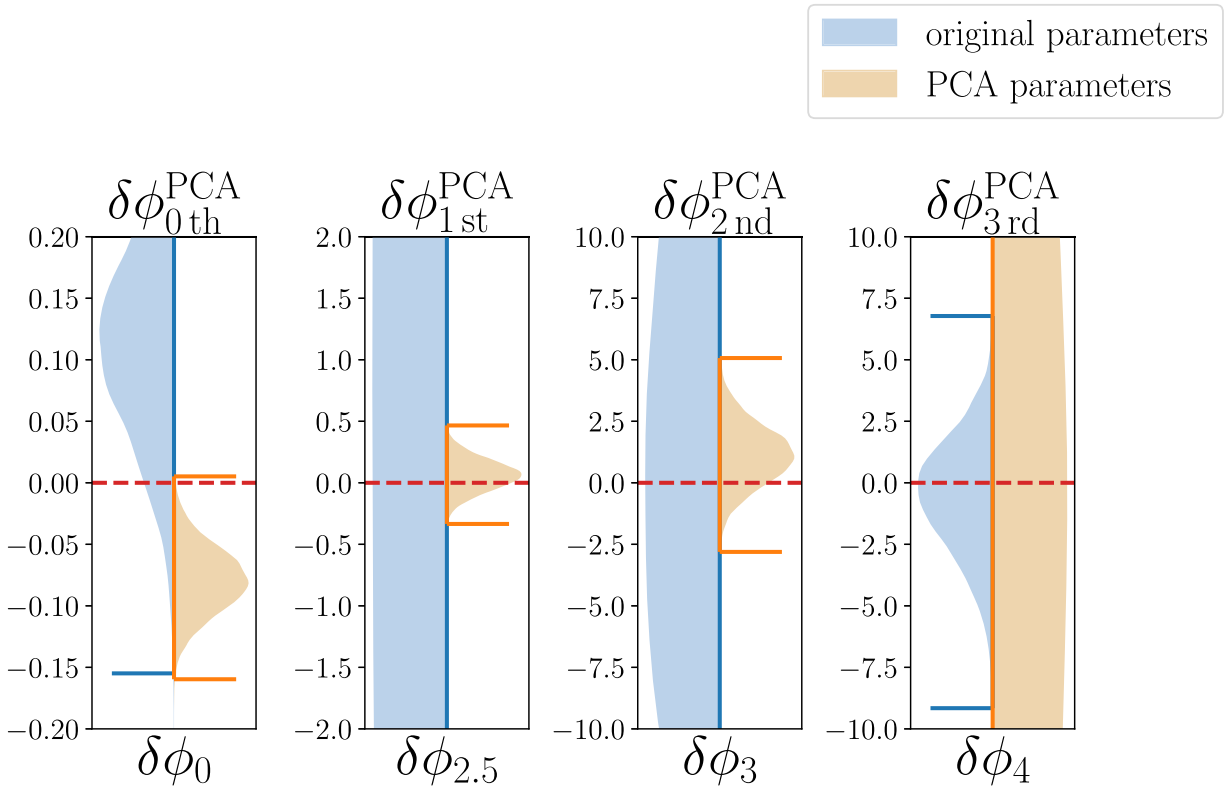

Figure 1. Posteriors of deformation parameters before and after performing PCA. The result shown here is obtained by combining posteriors of all selected events and averaging with weights of evidence for different waveform templates. The posteriors of original dispersion parameters are shown on the left side with blue shadows, and posteriors of PCA parameters are shown on the right side with orange shadows. The solid lines signify 99.7% credible intervals and the red dashed lines mean GR values.

Table 3
99.7% Credible Intervals and Distance between GR Values and Maximum Likelihood Values of Combined Results for Original Dispersion Parameters and PCA Parameters

Original Dispersion Parameters			PCA Parameters		
	99.7% Credible Interval	GR Value At		99.7% Credible Interval	GR Value At
$\delta\phi_0$	[−0.154, 0.363]	-1.34σ	$\delta\phi^{\rm PCA}_{0-\rm th}$	[−0.159 0.005 20]	2.85σ
$\delta\phi_{2.5}$	[−65.1, 57.9]	-0.0112σ	$\delta\phi^{\rm PCA}_{1-\rm st}$	[−0.334 0.466]	-0.480σ
$\delta\phi_3$	[−41.2, 50.9]	-0.0662σ	$\delta\phi^{\rm PCA}_{2-\rm nd}$	[−2.80 5.06]	-0.889σ
$\delta\phi_4$	[−9.15, 6.77]	0.190σ	$\delta\phi^{\rm PCA}_{3-\rm rd}$	[−71.3 83.0]	-0.0181σ

Note. The dominant PCA parameters can be better measured and constrained, thus having smaller error bars. The operation of PCA will make the behavior of deviating from zero in posteriors more obvious by transforming posterior samples into the set of new bases.

increases the demand for waveform accuracy when implementing the method of PCA.

However, the most common reason that induces the deviation is the insufficient accuracy of the waveform model, and the different results given by different waveform models also hint that. Other researches also encounter similar deviations and attribute the deviations to possible systematic errors. For example, see the discussion in Appendix C of Collaboration et al. (2021), and Appendix A of Perkins et al. (2021). It cannot be strictly proven that the deviation is indeed and only induced by systematic errors of waveform models. For example, the inclusion of effects of higher modes and precession in the waveform model `IMRPhenomXPHM` may help to break degeneracy among parameters which can allow us to get better measurements of source parameters. While this also increases the sensitivity of non-stationary and non-Gaussian features in the noise realization which are also potential reasons to induce bias in parameter estimation, it

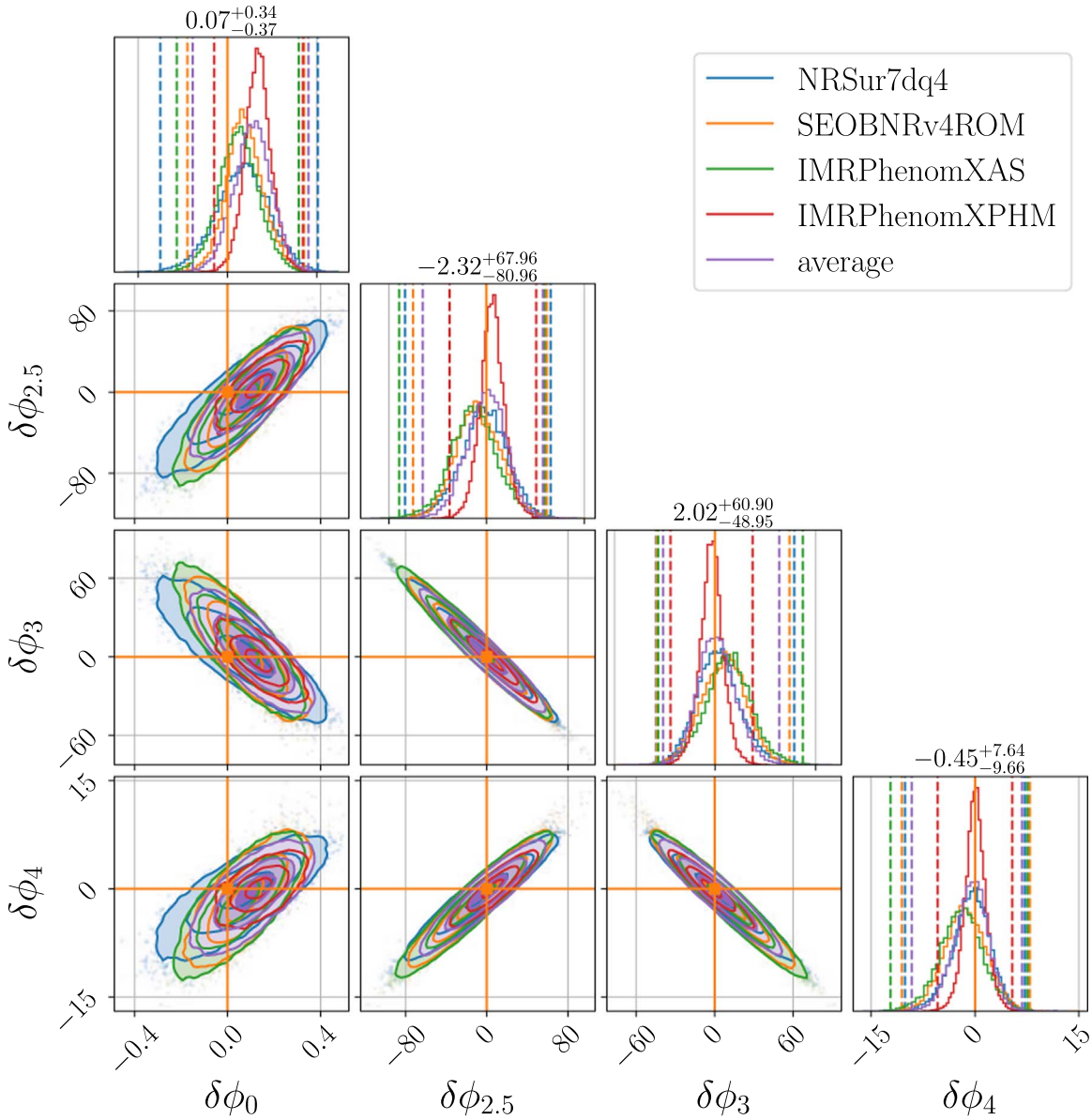

Figure 2. Posteriors of original dispersion parameters, which are combined results of all selected events, obtained by using different waveform models. The orange solid lines signify GR values and the dashed lines mean 99.7% credible intervals.

requires more thorough research in the future to exclude other possible reasons in parameter estimation and data processing.

4. Summary

GW observations have opened a new era of exploring the nature of the universe. Detected GW events have been leading paradigm-shifting in research of astrophysics, cosmology, and gravity. As the launch of the fourth observing run of LVK, it is expected that more GW events will be detected and more amazing discoveries may be revealed. GW observations provide a new approach to test gravity theories. Testing gravity with GWs has begun to blossom since the first GW event detection in 2015. Using detected events, LVK has performed exhaustive tests of GR (Collaboration et al. 2021, 2023, 2021c). Except for the theory-agnostic tests performed by LVK, theory-specific tests also have been performed by many independent research groups, such as (Jana & Mohanty 2019; Ramos & Barausse 2019; Wang et al. 2021a; Perkins et al. 2021; Gong et al. 2022; Wu et al. 2022; Haegel et al. 2023).

In this work, we consider the test of the GW dispersion relation which is conventionally performed by LVK. But in tests of LVK, to avoid the correlations among deformation

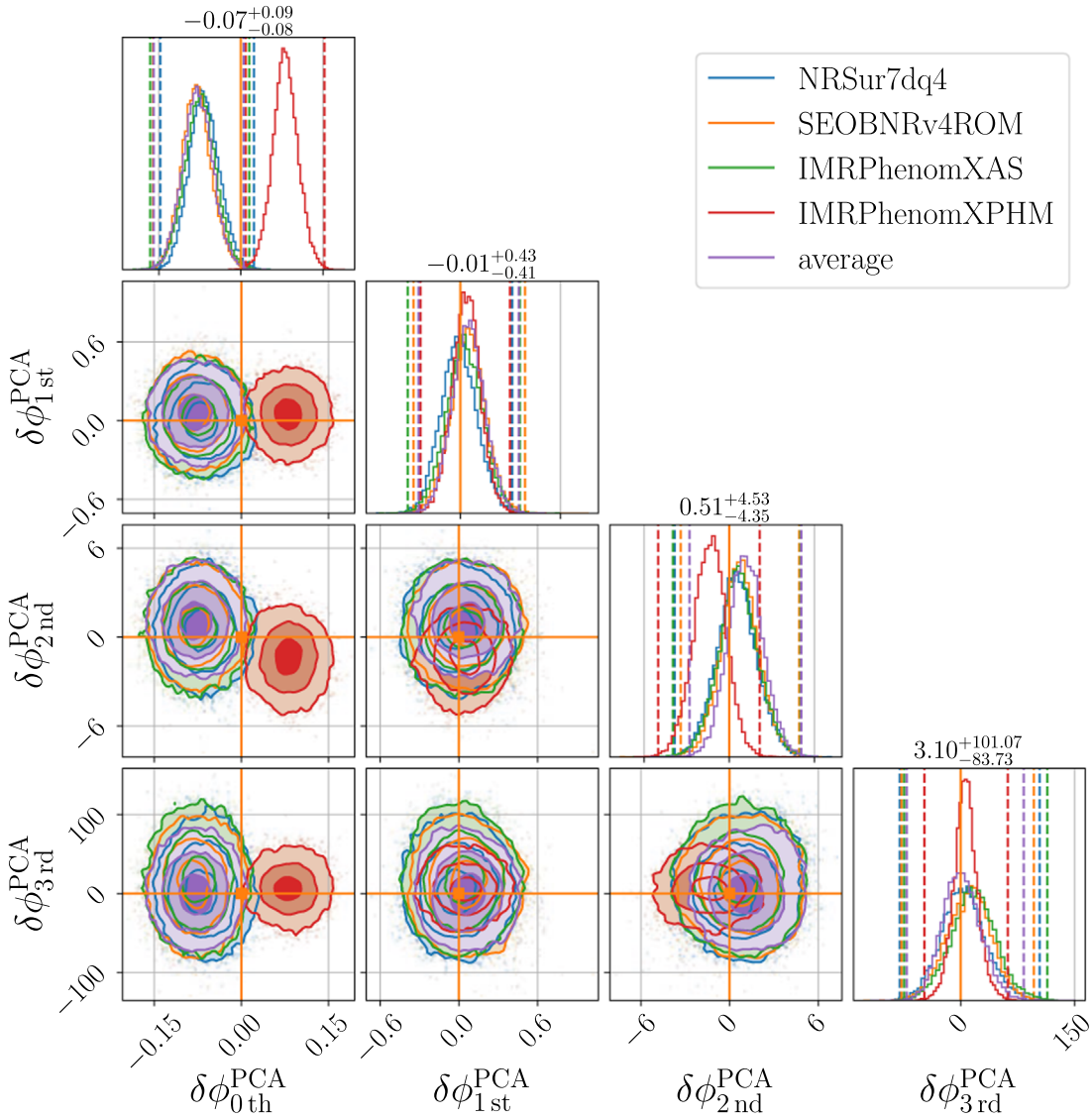

Figure 3. The results of applying PCA on the posteriors shown in Figure 2. Same as Figure 2, the orange solid lines signify GR values and dashed lines mean 99.7% credible intervals. Comparing with Figure 2, we can find that correlations among these parameters are reduced, and the first three dominant components are better constrained. We can also observe that the slight difference in posteriors of original dispersion parameters can lead to significant differences in results after applying PCA, especially in the first component, which hints that the multi-parameter test with PCA may require higher accuracy of waveform templates. Although the most common reason to induce the deviation is the insufficient accuracy of the waveform model, as discussed in Appendix C of Collaboration et al. (2021) and Appendix A of Perkins et al. (2021). It cannot be strictly proven that the deviation is indeed and only induced by systematic errors of waveform models. This requires more thorough research in the future to exclude other possible reasons in parameter estimation and data processing.

parameters to yield uninformative posteriors, only one deformation parameter is varied at a time. This is equivalent to considering the prior of the δ function for the fixed parameters. If considering the most agnostic prior, all deformation parameters need to be estimated simultaneously. Previous works (Pai & Arun 2012; Ohme et al. 2013; Saleem et al. 2022; Datta et al. 2024; Datta 2023; Shoom et al. 2023) show that the correlations can be reduced by the method of PCA. Using this method, the authors considered the parameterized test of PN structure where multiple deformation parameters are allowed to vary simultaneously, but still obtain informative posteriors meanwhile. We extend this method to the test of GW dispersion relation in this work.

The biggest difference in our analyses comparing with the tests of LVK is that the multiple dispersion parameters are varied simultaneously in Bayesian parameter estimation. Then we transform the obtained posterior samples into a set of new bases constructed by the PCA. The new PCA parameters have

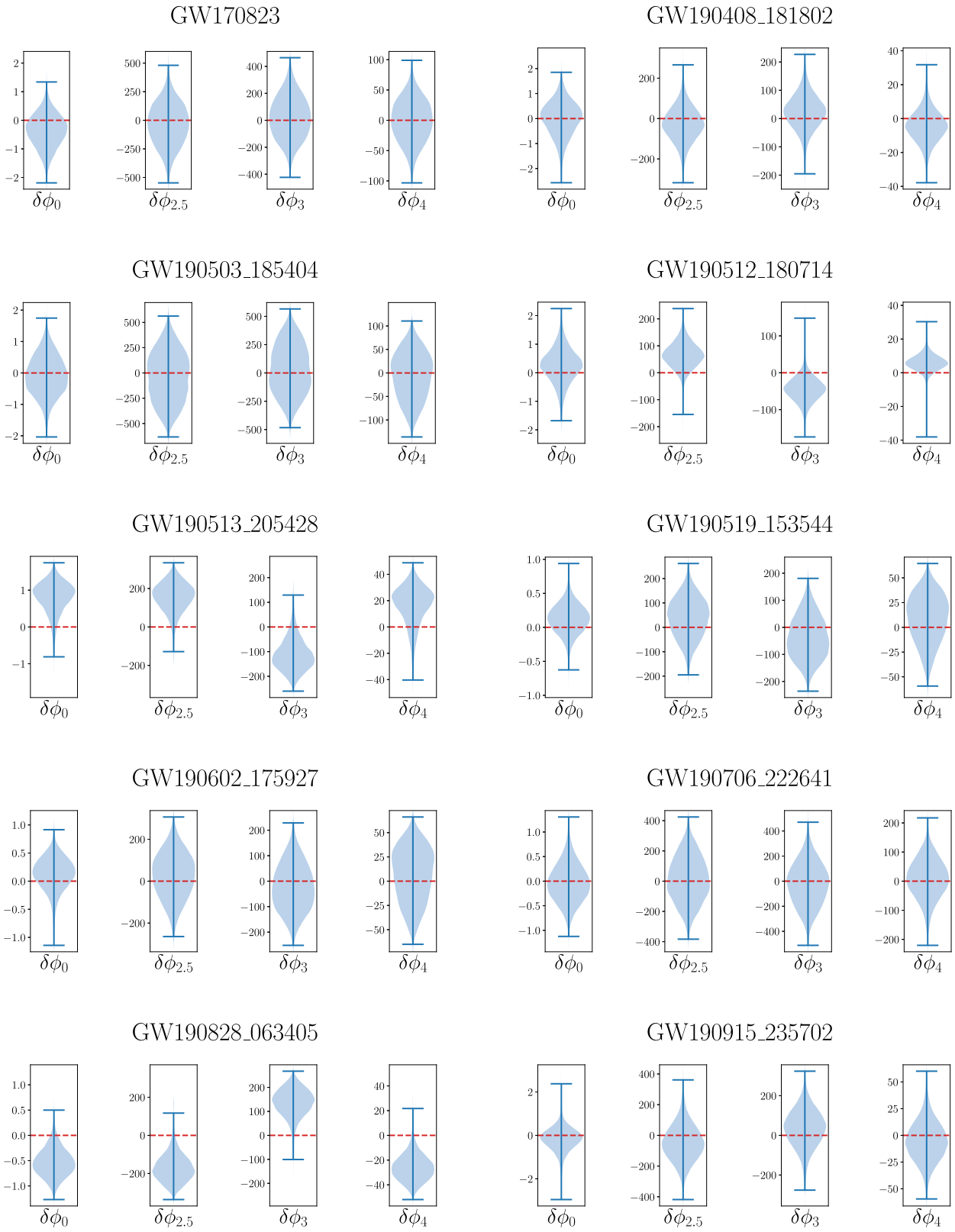

Figure 4. Posterior distributions of original dispersion parameters for each selected event. GR values are signified by red dashed lines, and 99.7% credible intervals are indicated by blue solid lines. The results shown here have been averaged with the weights of evidence of different waveform models.

less correlations, and dominant PCA parameters can be better measured and constrained, and thus are expected to be more sensitive to potential deviations from GR. We consider 10 farthest events selected by criteria of FAR $< 10^{-3}\,\mathrm{yr}^{-1}$, S/N > 12, and $p_{\mathrm{astro}} > 0.99$. We consider four different GR waveforms and add the modifications of the dispersion effect into them as the template in Bayesian parameter estimation. The results we obtain are consistent with GR within 99.7% credible intervals in all cases. However, we observe that the maximum likelihood value of the first PCA parameter has a relatively large departure from the GR value. This on the one hand shows the dominant PCA parameter is more sensitive to deviations from zero in posteriors, and on the other hand hints that the demand of waveform accuracy is higher when using PCA. We also find that minor differences in posteriors of original parameters can lead to obvious differences in results after the operation of PCA, which from another aspect indicates multi-parameter tests with PCA require more accurate waveform models. Although the systematic errors of waveform models are the most common reason to induce deviations, it cannot be strictly proven that the deviation is indeed and only induced by systematic errors. The non-stationary and non-Gaussian features in the noise realization are also potential reasons to induce bias in parameter estimation. This requires more thorough research in the future to exclude other possible reasons in parameter estimation and data processing.

Acknowledgments

W.Z. is supported by the National Key R&D Program of China (grant No. 2022YFC2204602 and 2021YFC2203102), Strategic Priority Research Program of the Chinese Academy of Science (grant No. XDB0550300), the National Natural Science Foundation of China (NSFC, Grant Nos. 12325301 and 12273035), the Fundamental Research Funds for the Central Universities (grant No. WK2030000036 and WK3440000004), the Science Research Grants from the China Manned Space Project (grant No. CMS-CSST-2021-B01), and the 111 Project for “Observational and Theoretical Research on Dark Matter and Dark Energy” (grant No. B23042). R.N. is supported in part by the National Key Research and Development Program of China grant No.2022YFC2807303.

This research has made use of data or software obtained from the Gravitational Wave Open Science Center (gwosc.org), a service of the LIGO Scientific Collaboration, the Virgo Collaboration, and KAGRA. This material is based upon work supported by NSF’s LIGO Laboratory which is a major facility fully funded by the National Science Foundation, as well as the Science and Technology Facilities Council (STFC) of the United Kingdom, the Max-Planck-Society (MPS), and the State of Niedersachsen/Germany for support of the construction of Advanced LIGO and construction and operation of the GEO600 detector. Additional support for Advanced LIGO was provided by the Australian Research Council. Virgo is funded, through the European Gravitational Observatory (EGO), by the French Centre National de Recherche Scientifique (CNRS), the Italian Istituto Nazionale di Fisica Nucleare (INFN) and the Dutch Nikhef, with contributions by institutions from Belgium, Germany, Greece, Hungary, Ireland, Japan, Monaco, Poland, Portugal, and Spain. KAGRA is supported by Ministry of Education, Culture, Sports, Science and Technology (MEXT), Japan Society for the Promotion of Science (JSPS) in Japan; National Research Foundation (NRF) and Ministry of Science and ICT (MSIT) in Korea; Academia Sinica (AS) and "National Science and Technology Council" (NSTC) in Taiwan, China.

The numerical calculations in this paper have been done on the supercomputing system in the Supercomputing Center of University of Science and Technology of China. Data analyses and results visualization in this work made use of `Bilby` (Ashton et al. 2019), `Pymultinest` (Feroz & Hobson 2007; Feroz et al. 2008; Buchner et al. 2014), `LALSuite` (LIGO Scientific Collaboration 2018), `PESummary` (Hoy & Raymond 2021), `NumPy` (van der Walt et al. 2011; Harris et al. 2020), `Scipy` (Virtanen et al. 2020), and `matplotlib` (Hunter 2007).

References

Abbott, B., Abbott, R., Abbott, T., et al. 2016a, PhRvL, 116, 061102 Abbott, B., Abbott, R., Abbott, T., et al. 2016b, PhRvL, 116, 221101 Abbott, B., Abbott, R., Abbott, T., et al. 2019a, PhRvX, 9, 031040
Abbott, B., Abbott, R., Abbott, T., et al. 2019b, PhRvL, 123, 011102 Abbott, B., Abbott, R., Abbott, T., et al. 2019c, PhRvD, 100, 104036 Abbott, B. P., Abbott, R., Abbott, T. D., et al. 2020, CQGra, 37, 055002 Abbott, R., Abbott, T. D., Abraham, S., et al. 2021, PhRvX, 11, 021053 Adelberger, E. G. 2001, CQGra, 18, 2397
Agathos, M., Pozzo, W. D., Li, T., et al. 2014, PhRvD, 89, 082001
Aghanim, N., Akrami, Y., Ashdown, M., et al. 2020, A&A, 641, A6
Amelino-Camelia, G. 2002, Nature, 418, 34
Ashton, G., Hübner, M., Lasky, P. D., et al. 2019, ApJS, 241, 27
Ashton, G., & Khan, S. 2019, PhRvD, 101, 064037
Belgacem, E., Dirian, Y., Foffa, S., & Maggiore, M. 2018, PhRvD, 97, 104066
Berti, E., Barausse, E., Cardoso, V., et al. 2015, CQG, 32, 243001 Buchner, J., Georgakakis, A., Nandra, K., et al. 2014, A&A, 564, A125 Calcagni, G. 2010, PhRvL, 104, 251301
Collaboration, T. L. S., the Virgo Collaboration, Abbott, R., et al. 2021, PhRvD, 103, 122002
Collaboration, T. L. S., the Virgo Collaboration, Abbott, R., et al. 2021a, arXiv:2108.01045
Collaboration T. L. S., the Virgo Collaboration, the KAGRA Collaboration, et al. 2023, PhRvX, 13, 041039
Collaboration T. L. S., the Virgo Collaboration, the KAGRA Collaboration, et al. 2021c, arXiv:2112.06861
Cornish, N. J., & Littenberg, T. B. 2015, CQGra, 32, 135012
Datta, S. 2023, arXiv:2303.04399
Datta, S., Gupta, A., Kastha, S., Arun, K. G., & Sathyaprakash, B. S. 2021, PhRvD, 103, 024036
Datta, S., Saleem, M., Arun, K. G., & Sathyaprakash, B. S. 2024, PhRvD, 109, 044036
Debono, I., & Smoot, G. 2016, Universe, 2, 23
DeWitt, B. S. 1967, PhRv, 160, 1113
Feroz, F., & Hobson, M. P. 2007, MNRAS, 384, 449
Feroz, F., Hobson, M. P., & Bridges, M. 2008, MNRAS, 398, 1601

Foreman-Mackey, D., Hogg, D. W., Lang, D., & Goodman, J. 2013, PASP, 125, 306
Frieman, J. A., Turner, M. S., & Huterer, D. 2008, ARA&A, 46, 385
Ghosh, A., Ghosh, A., Johnson-McDaniel, N. K., et al. 2016, PhRvD, 94, 021101
Ghosh, A., Johnson-McDaniel, N. K., Ghosh, A., et al. 2017, CQGra, 35, 014002
Gong, C., Zhu, T., Niu, R., et al. 2022, PhRvD, 105, 044034
Gupta, A., Datta, S., Kastha, S., et al. 2020, PhRvL, 125, 201101
Haegel, L., O'Neal-Ault, K., Bailey, Q. G., et al. 2023, PhRvD, 107, 064031
Harris, C. R., Millman, K. J., van der Walt, S. J., et al. 2020, Nature, 585, 357
Hastings, W. K. 1970, Biometrika, 57, 97
Hořava, P. 2009, PhRvD, 79, 084008
Hoy, C., & Raymond, V. 2021, SoftwareX, 15, 100765
Hoyle, C. D., Schmidt, U., Heckel, B. R., et al. 2001, PhRvL, 86, 1418
Hunter, J. D. 2007, CSE, 9, 90
Jain, B., & Khoury, J. 2010, AnPhy, 325, 1479
Jana, S., & Mohanty, S. 2019, PhRvD, 99, 044056
Kiefer, C. 2007, Approaches to Fundamental Physics (Berlin: Springer), 123
Kostelecký, V. A., & Mewes, M. 2016, PhLB, 757, 510
Koyama, K. 2016, RPPh, 79, 046902
Kramer, M. 2017, The Fourteenth Marcel Grossmann Meeting (Singapore: World Scientific)
Li, T. G. F., Pozzo, W. D., Vitale, S., et al. 2012, PhRvD, 85, 082003
LIGO Scientific Collaboration 2018, LIGO Algorithm Library - LALSuite, free Software (GPL), doi:10.7935/GT1W-FZ16
Manchester, R. N. 2015, IJMPD, 24, 1530018
Mirshekari, S., Yunes, N., & Will, C. M. 2012, PhRvD, 85, 024041
Nishizawa, A. 2018, PhRvD, 97, 104037
Niu, R., Ma, Z.-C., Chen, J.-M., Feng, C., & Zhao, W. 2024, ResPh, 57, 107407
Niu, R., Zhu, T., & Zhao, W. 2022, JCAP, 2022, 011
Ohme, F., Nielsen, A. B., Keppel, D., & Lundgren, A. 2013, PhRvD, 88, 042002
Okounkova, M., Farr, W. M., Isi, M., & Stein, L. C. 2021, PhRvD, 106, 044067
Pai, A., & Arun, K. G. 2012, CQGra, 30, 025011
Perkins, S. E., Nair, R., Silva, H. O., & Yunes, N. 2021, Phys. Rev. D, 104, 024060
Porter, T. A., Johnson, R. P., & Graham, P. W. 2011, ARA&A, 49, 155
Pratten, G., García-Quirós, C., Colleoni, M., et al. 2021, PhRvD, 103, 104056
Pratten, G., Husa, S., García-Quirós, C., et al. 2020, PhRvD, 102, 064001
Pürrer, M. 2014, CQGra, 31, 195010
Pürrer, M. 2015, PhRvD, 93, 064041
Ramos, O., & Barausse, E. 2019, PhRvD, 99, 024034
Romero-Shaw, I. M., Talbot, C., Biscoveanu, S., et al. 2020, MNRAS, 499, 3295
Saleem, M., Datta, S., Arun, K. G., & Sathyaprakash, B. S. 2022, PhRvD, 105, 084062
Sefiedgar, A., Nozari, K., & Sepangi, H. 2011, PhLB, 696, 119
Shoom, A. A., Gupta, P. K., Krishnan, B., Nielsen, A. B., & Capano, C. D. 2023, GReGr, 55, 55
Skilling, J. 2004, in AIP Conf. Proceedings (Melville, NY: AIP) Conf. Proceedings (AIP)AIP, 35
Skilling, J. 2006, BayAn, 1, 833
Stairs, I. H. 2003, LRR, 6, 5
van der Walt, S., Colbert, S. C., & Varoquaux, G. 2011, CSE, 13, 22
Varma, V., Field, S. E., Scheel, M. A., et al. 2019, PhRvR, 1, 033015
Virtanen, P., Gommers, R., Oliphant, T. E., et al. 2020, NatMe, 17, 261
Wang, Y.-F., Brown, S. M., Shao, L., & Zhao, W. 2021a, PhRvD, 106, 084005
Wang, Y.-F., Brown, S. M., Shao, L., & Zhao, W. 2022, PhRvD, 106, 084005
Wang, Y.-F., Niu, R., Zhu, T., & Zhao, W. 2021b, ApJ, 908, 58
Wex, N. 2014, arXiv:1402.5594
Will, C. M. 1998, PhRvD, 57, 2061
Will, C. M. 2014, LRR, 17, 4
Wu, Q., Zhu, T., Niu, R., Zhao, W., & Wang, A. 2022, PhRvD, 105, 024035
Yunes, N., & Pretorius, F. 2009, PhRvD, 80, 122003
Yunes, N., Yagi, K., & Pretorius, F. 2016, PhRvD, 94, 084002
Zhao, W., Zhu, T., Qiao, J., & Wang, A. 2020, PhRvD, 101, 024002